PAPER

Recycling of NdFeB magnets employing oxidation, selective leaching, and iron precipitation in an autoclave

Elif Emil-Kaya, [ID] *[abc] Buse Polat,[a] Srecko Stopic,[a] Sebahattin Gürmen[b] and Bernd Friedrich [ID] [a]

The increasing production of neodymium–iron–boron (NdFeB) magnets for technological applications results in disposal problems. NdFeB magnets contain a significant quantity of rare earth elements (REEs). China is the largest REEs producer, but it applies quotas and increases the export prices of REEs. To address this issue, this study aims at investigating the recovery process of REEs from scrap NdFeB magnets. After oxidation of NdFeB magnet powders, selective leaching with nitric acid was carried out to achieve high-purity REE-rich leaching liquor. First, the oxidation kinetics of NdFeB powders was studied in detail to determine the oxidation temperature and duration. Afterwards, the effects of selective leaching parameters, including acid concentration, leaching temperature, stirring speed and solid/liquid ratio, were examined by analysis of variance (ANOVA) analysis based on Taguchi method. The most substantial parameters were assigned to be the temperature and solid/liquid ratio. Eventually, the dissolution kinetics were studied to propose a model for REEs. Several universal equations for dissolution kinetics were tested, and $(1 - (1 - x) = k \times t^n)$ gives the best results for REEs. The findings show that the leaching process follows the shrinking core model. Activation energy was calculated to be 40.375 kJ mol^{-1} for REEs. As the last step, the iron dissolved during leaching was precipitated as hematite in the autoclave. The hematite precipitation experiments were performed based on the Box–Behnken design. The effect of precipitation parameters was investigated by ANOVA analysis, and the precipitation process was optimized using response surface methodology (RSM), which resulted in the minimum iron and maximum REEs content in the leach liquor.

Introduction

Permanent magnets and rare earth elements (REEs) have wide usage in technological products and applications and form the basis for a new generation of technology. However, REEs were added to the list of critical metals due to the increased demand and the associated supply risk.[1–3] REEs are the ones with the highest supply risk among all elements, and are on the list of critical metals in Europe. The critical importance of permanent magnets and REEs led to an increase in efforts to ensure the sustainability of their raw materials. The importance of NdFeB magnets in technological applications and the inclusion of REEs in the list of critical metals led to a search for alternative ways to obtain raw materials.[4–6] NdFeB magnets are used in a wide variety of high-tech products; therefore, the recycling of

NdFeB magnets whose service life is completed or which are scrapped due to a process error is the most effective alternative solution to the supply problem of raw materials.[7–9] There have been plenty of studies on the recovery of REEs using pyrometallurgy and hydrometallurgy.[10–18] The widely preferred technique for recovering REEs from waste materials is hydrometallurgy. Hydrometallurgical processes can produce pure products from lower grade and complex streams. In addition, compared to the pyrometallurgical route, the leaching process, which produces less gas emission, may be carried out more simply and scaled up with lower operational costs.[19–21]

Kumari *et al.* studied the selective leaching of Nd, Pr and Dy from NdFeB magnets of wind turbines. Roasted magnet powders were leached to define optimum leaching parameters. The optimum leaching conditions of 0.5 mol L^{-1} HCl, 100 g L^{-1} pulp density, 368 K temperature and 500 rpm stirring speed were determined for achieving 98% purity of REEs. The dissolution kinetics of REEs follow the mixed controlled model in the range of 348 to 368 K. Finally, mixed RE oxides of 99% purity were produced using oxalic acid followed by calcination at 1073 K.[22] The effects of solid/liquid ratio, stirring speed, time, temperature, acid type and acid concentration on the selective

[a] *IME Process Metallurgy and Metal Recycling, RWTH Aachen University, Aachen 52056, Germany. E-mail: eemil@ime-aachen.de*

[b] *Department of Metallurgical & Materials Eng., Istanbul Technical University, Istanbul 34469, Turkey*

[c] *Department of Materials Science and Tech., Turkish-German University, Istanbul 34820, Turkey*

leaching process of REEs from waste NdFeB magnets were investigated based on the L18 Taguchi orthogonal array by Ni'am *et al.* Acid type is the most important factor for the selective leaching process of magnets, and leaching of the oxidized sample with 5 mol L^{-1} HCl at 368 K and 2% solid–liquid ratio for 24 h allows selective recovery of REEs.[23] Jiang *et al.* reported that magnet powders roasted at 800 °C were leached under pressure, with the REEs leaching rate of 96.27%, along with 13.33% for Fe. After the water leaching, hematite was separated from the leach liquor. The selective pressure HCl acid leaching process for NdFeB magnets was evaluated in detail.[24]

Yoon *et al.* proposed a leaching mechanism for NdFeB magnets, and the activation energy was calculated. Nd and Nd_2O_3 in the NdFeB magnet was converted to $Nd_2(SO_4)_3$ in solution with 3 mol L^{-1} H_2SO_4 and a pulp density of 110.8 g L^{-1} for 4 h. It was reported that the leaching kinetics followed a shrinking core model.[25] Liu *et al.* studied the selective separation of REEs from iron by a selective pressure leaching process. In this study, REEs and Boron were effectively separated from the iron, especially with the addition of $NaNO_3$ promoter to decrease the level of iron in the leaching solution. Afterwards, boron was recovered by the solvent extraction process.[26] In another study reported by Mao *et al.*, the effect of mechanical activation of oxidized magnet powder on the efficiency of selective leaching process by low-concentration HCl was investigated. The reactivity of magnet powder increased with ball milling activation. It enhanced the leaching speed and leaching efficiency of REEs.[27] Considering the studies in the literature, selective leaching of NdFeB with HNO_3 was not investigated in detail. In addition, hematite precipitation is a well-known method in hydrometallurgy, but it is still an outstanding topic for the recycling of NdFeB magnets.

Dutricaz *et al.* investigated hematite precipitation from ferric chloride at a temperature less than 100 °C at atmospheric pressure. The formation of β-FeO·OH was observed at approximately 60 °C by controlling the seeding and changing the molarity of the solution. Prolonged retention time favored a stable hematite phase, at times longer than 100 h, where only hematite phase was observed.[28] In the zinc industry, the hematite precipitation process has been employed for the iron removal process. Cheng *et al.* elucidated the kinetics and chemistry of hematite precipitation. In their study, hematite was formed through the oxydrolysis reaction of ferrous sulphate at temperatures between 195 and 200 °C at a pressure in the range of 103 to 414 kPa.[29]

The aim of this work to was examine the oxidation of NdFeB magnet powders and their selective leaching and hematite precipitation in the autoclave. The leaching optimization and kinetics study on the dissolution of REEs from NdFeB magnet powders with nitric acid for the functions of solid/liquid ratio, acid concentration, stirring speed and temperature were investigated based on the experimental design method and statistical analysis. Afterwards, the influence of temperature, time and water addition on the precipitation of iron and REEs in the autoclave was examined by ANOVA analysis on the basis of Box–Behnken experimental design. Moreover, the effect of process parameters and their relationship on the iron and REEs

precipitation are investigated *via* response surface methodology.

Experimental

Scrap NdFeB magnet powder and oxidized powder characterization

Waste NdFeB magnet samples were supplied in bulk form. The samples were crushed to obtain suitable particle size for leaching experiments using a jaw crusher (Retsch GmbH, Haan, Germany); subsequently, the powders were sieved with a vibratory sieve shaker (Retsch, AS200). X-ray fluorescence (XRF) spectroscopy (Panalytical WDXRF spectrometer, Malvern Panalytical B.V., Eindhoven, Netherlands) and inductively coupled plasma optical emission spectroscopy ICP-OES (SPECTRO ARCOS, SPECTRO Analytical Instruments GmbH, Kleve, Germany) analyses were conducted to determine the elemental composition of NdFeB magnet powders.

Oxidation of NdFeB magnet powders

The oxidation of NdFeB magnet powders was performed in a muffle furnace. The experiments for calculation of weight gain were implemented by heating 1 g of magnet powder in an alumina crucible in a muffle furnace. After the furnace reached each desired temperature, 1 g of sample was placed into the hot zone of the muffle furnace and held in ambient air for the desired durations. Afterwards, the samples were weighed, and graphs of the weight gain *versus* time were drawn. On the basis of the graphs of weight gain – time and the DTA-TG analysis, the optimum oxidation temperature was determined. Phase analysis of the oxidized magnet powders was carried out with the LynxEye detector, applying Cu-Kα radiation ($\lambda = 1.54187$ Å) in the X-ray diffractometer (Bruker D8 Advance) in the 2θ range of 10–90°. To reveal the particle size distribution of the oxidized magnet powders, dynamic particle analysis was conducted with an M5 lens by SympaTech QuickPick Oasis. The morphology of the oxidized NdFeB magnet powders was by revealed scanning electron microscope (Zeiss Gemini 500).

Taguchi experimental design for selective leaching with HNO_3

Selective leaching experiments were conducted in a 500 mL three-neck round-bottom glass flask placed on a heating mantle (IKA Werke GmbH, Staufen im Breisgau, Germany) equipped with temperature controller. Nitric acid (65%) was provided by VWR International GmbH, Darmstadt, Germany in analytical grade.

One neck of the flask is attached with the probe for the temperature controller; the other neck is used to attach with a condenser; and the other neck is used for feeding and withdrawing the samples during the leaching process at defined time intervals. The leaching solution in the flask was stirred using a mechanical stirrer at a variable speed for 3 h. A Teflon stirrer blade was preferred for the stirring of the solution. The schematic experimental setup for the selective leaching process is exhibited in Fig. 1.
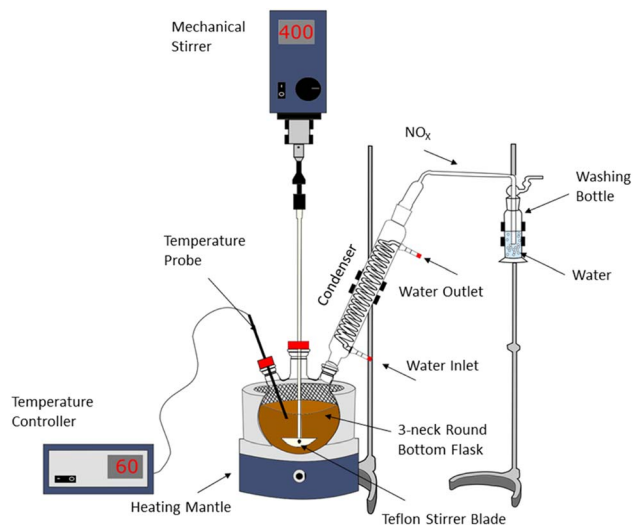
Fig. 1 Schematic picture of experimental setup for selective leaching experiments.

Table 1 The experimental parameters for selective leaching

Parameters	Levels		
	1	2	3
Acid concentration (mol L^{-1})	1	2	3
Solid : liquid ratio	1/10	1/20	1/30
Process temperature (°C)	40	60	80
Stirring speed (rpm)	200	350	500

To establish the best experimental conditions for the selective leaching process of NdFeB magnets by nitric acid, Taguchi orthogonal array (L9) was employed. The orthogonal array was composed of 4 variables with 3 levels each. The process parameters and their levels for selective leaching can be found in Table 1.

After the optimum process parameters were defined by using the Taguchi plots, the leaching process was analysed using several kinetic models at different leaching temperatures.

After selective dissolution of REEs, leach solution was filtered by vacuum filtration setup. After filtration, the pregnant leach solutions were sampled to elucidate the dissolution of REEs and iron. Potentiometric titration of Fe^{2+} in the solution was performed with cerium(IV) sulfate using a titration system (Metrohm Dosimat 655, Titrosampler 855). Finally, the kinetic calculation was performed to define the leaching control mechanism of REEs and iron.

Box–Behnken design for hematite precipitation in the autoclave

During selective leaching process, iron dissolution was observed. The dissolved iron was precipitated in the autoclave. Fig. 2 illustrates the schematic diagram of the autoclave.

Before precipitation experiments, some preliminary experiments for iron precipitation in the autoclave were performed.
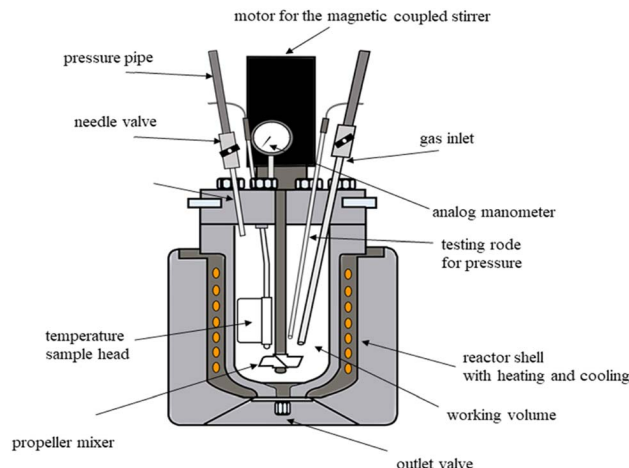

Fig. 2 Schematic diagram of the autoclave.

Table 2 Process parameters and their levels for Box–Behnken Design

Parameters	Levels		
	1	2	3
Process temperature (°C)	140	160	180
Time (h)	2	4	6
Water addition (%)	0	25	50

However, the precipitation ratio of iron was found to be low based on the result of preliminary experiments. Before the iron precipitation in the autoclave, with the aim of removal of iron from the system, the pH value of the leach solution was increased by adding NH$_4$OH until it reached approximately 1. After that, the pH value of the solutions with water addition of 0%, 25%, and 50% were measured. The pH value of the solutions were approximately 1, 1.2, and 1.4, respectively.

A Box–Behnken design was employed for the iron removal process in an autoclave under pressure. The precipitation experiments in the autoclave were conducted with three parameters in three levels. Process temperature was adjusted in three levels of 140, 160, and 180 °C, process time of 2, 4, and 6 h, and water addition of 0, 25 and 50%. The process parameters and their levels can be found in Table 2.

Afterwards, Taguchi and ANOVA analyses were conducted to define the optimal process conditions. Optimization tool in MINITAB was employed to specify the optimal process parameters for achieving both maximum REEs extraction and minimum iron extraction.

Results and discussion

Characterization of NdFeB magnet powders

The composition of NdFeB magnet powder was determined using XRF. Table 3 shows the phase composition of NdFeB magnet powder. As can be seen in Table 3, the presence of Fe, Nd and Pr, as well as small amounts of Dy, Al, Si, Co, Mn, and

Paper

Table 3 Chemical phase of NdFeB magnet powder determined by XRF analysis

Component	Na_2O	Al_2O_3	SiO_2	MnO	Fe_2O_3
Concentration (%)	0.34	0.42	0.24	1.97	68.1
Component	Co_3O_4	CuO	Ga_2O_3	As_2O_3	Nb_2O_5
Concentration (%)	0.70	0.14	0.20	0.21	0.12
Component	PdO	Pr_2O_3	Nd_2O_3	Tb_4O_7	Other
Concentration (%)	0.24	5.72	20.4	0.70	0.50

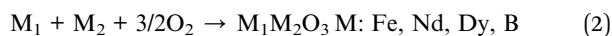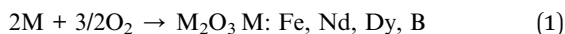**Table 4** Chemical analysis of NdFeB magnet powder determined by ICP analysis

Composition	B	Co	Cr	Cu	Dy
Concentration (%)	0.877	0.773	< 0.1	0.102	0.662
Composition	Fe	Mo	Nd	Ni	Pr
Concentration (%)	66.27	< 0.1	23.9	< 0.1	7.38
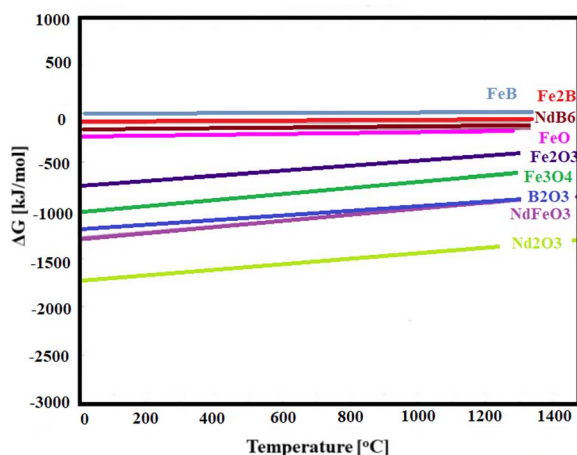
Fig. 3 Phase formation during oxidation of NdFeB magnets.

Pd, was detected with XRF analysis. The results of ICP-OES analysis of NdFeB magnet powders is shown in Table 4.
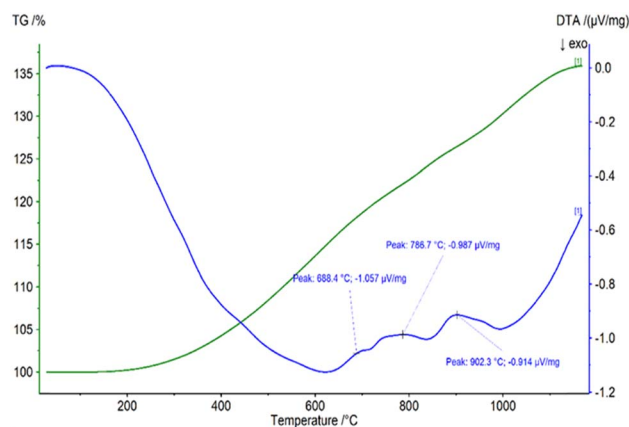
Oxidation of NdFeB magnet powders

During oxidation of the powder samples, various phases were observed in previous literature ($NdFeO_3$, $PrFeO_3$, Nd_2O_3). Analysis of Gibbs energy at different temperatures was investigated based on eqn (1) and (2):

$$2M + 3/2O_2 \rightarrow M_2O_3 \quad \text{M: Fe, Nd, Dy, B} \tag{1}$$

$$M_1 + M_2 + 3/2O_2 \rightarrow M_1M_2O_3 \quad \text{M: Fe, Nd, Dy, B} \tag{2}$$

Thermochemical calculation was used to predict the possible phase formation and its corresponding sequence, and this is shown in Fig. 3.

The figures demonstrated that the first phase to form will be Nd_2O_3 due to its most negative standard free enthalpy of formation ($\Delta G°$), following by $NdFeO_3$ and finishing with Fe_2B, as the line of FeB is slightly above 0, corresponding to a non-spontaneous reaction. Based on the composition of the raw

Fig. 4 DTA-TGA analysis of NdFeB magnet powders in air (10 K min^{-1}).

materials, the phases of Nd_2O_3, $NdFeO_3$ and Fe_xO_y are highly expected. Fig. 4 illustrates the DTA-TGA analysis of NdFeB magnet powders.

Because of an oxidation process, TGA analysis revealed an increased sample mass of about 35% between room temperature and 1100 °C, which is very close to the total calculated theoretical value (36.8%) for the oxidation of Fe, REEs and B. The calculated theoretical value for the oxidation of REEs amounts to 3.6%. DTA analysis revealed three peaks at 688, 786, and 902 °C, respectively, that show different types of oxide can be formed.

Firstly, to determine the oxidation temperature and time, magnet powders were oxidized at different temperatures for 15, 30, 45, 60, 75, 90, 120, 150 and 180 min. The weight gains of samples were calculated, and the graph of the weight gain and time were drawn, shown in Fig. 5.

On the basis of DTA-TGA analysis, 900, 1000 and 1100 °C were chosen as the oxidation temperature. The experiments at 120, 150 and 180 minutes were implemented twice in order to have more precise data. After the desired holding time was reached, samples were taken from the furnace and weighed immediately.

The values of weight gain were summed up and averaged. The oxidation temperature was determined to be 900 °C for 150 min.

Fig. 6 illustrates the XRD analysis of the oxidized magnet powders at 900 °C for 150 min.

According to the XRD analysis, the oxidized material consists entirely of the metal oxides. Through the oxidation, $Nd_2Fe_{14}B$ decomposed to form Fe_2O_3, Nd_2O_3 and $NdFeO_3$. The XRD peaks in Fig. 6 correspond to rhombohedral Fe_2O_3, orthorhombic $NdFeO_3$, hexagonal Nd_2O_3 with the space group of $R\bar{3}c$ (JCPDS #01-084-0307), $Pnma$ (JCPDS #01-089-6644) and $P\bar{3}m1$ (JCPDS #00-006-0408), respectively. Fig. 7 shows SEM images of the oxidized NdFeB magnet particles with EDS analysis.

The morphology of the oxidized NdFeB magnet powders was irregular, having a narrow size distribution. Furthermore, EDS analysis confirmed the presence of Nd, Fe, Pr, Dy and O. Fig. 8 shows the dynamic particle analysis of the NdFeB magnet powders.
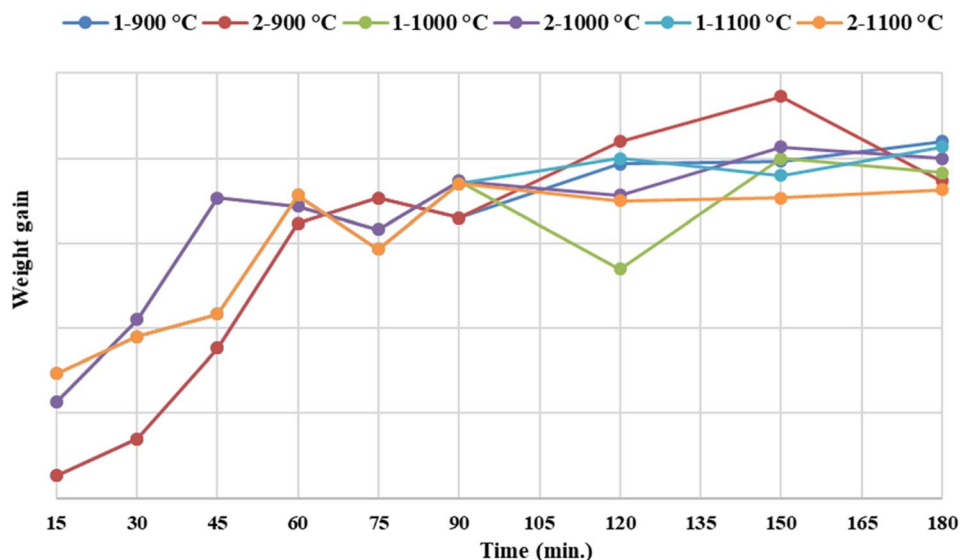
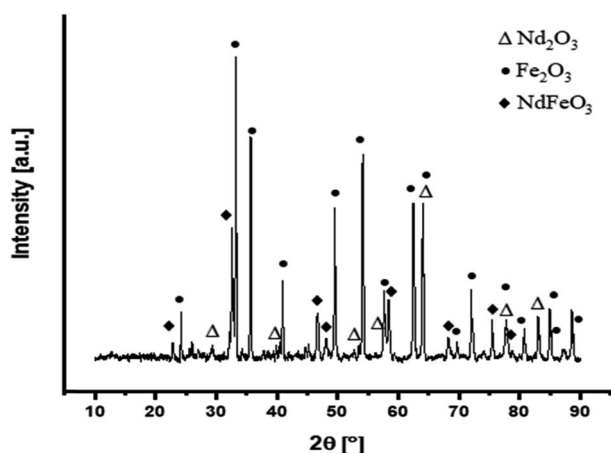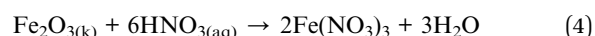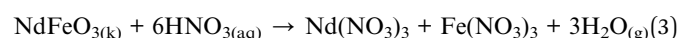Fig. 5 Graphic of the weight gain and time at 900, 1000 and 1100 °C.

Fig. 6 XRD analysis of the oxidized magnet powders at 900 °C for 150 min.

Fig. 8 reveals the distribution density (q_3^*) and cumulative distribution (Q_3) of the oxidized NdFeB magnet powders with the diameter (EQPC)-value of the NdFeB magnet powders.

According to the distribution sum (Q_3), the $d_{90.3}$, $d_{50.3}$, $d_{10.3}$ values are 92.62 μm, 64.04 μm and 5.96 μm, respectively. These results confirm that 90.3% of the oxidized NdFeB magnet powders range in size from 5.96 to 100 μm. The distribution density of powders (q_3^*) reaches its global maximum at ~80 μm.

Taguchi analysis of selective leaching process and statistical analysis

Considering the environmental factors, maximum leaching efficiency was aimed with minimum acid consumption for the design of the leaching experiments. Reactions for Nd and Fe (main components in waste NdFeB magnet) dissolution in HNO_3 are given in eqn (3) and (4).

$$NdFeO_{3(k)} + 6HNO_{3(aq)} \rightarrow Nd(NO_3)_3 + Fe(NO_3)_3 + 3H_2O_{(g)} \quad (3)$$

$$Fe_2O_{3(k)} + 6HNO_{3(aq)} \rightarrow 2Fe(NO_3)_3 + 3H_2O \quad (4)$$

The three-level L9 orthogonal array was employed to optimize the leaching efficiency of iron and REEs. Table 5 gives the
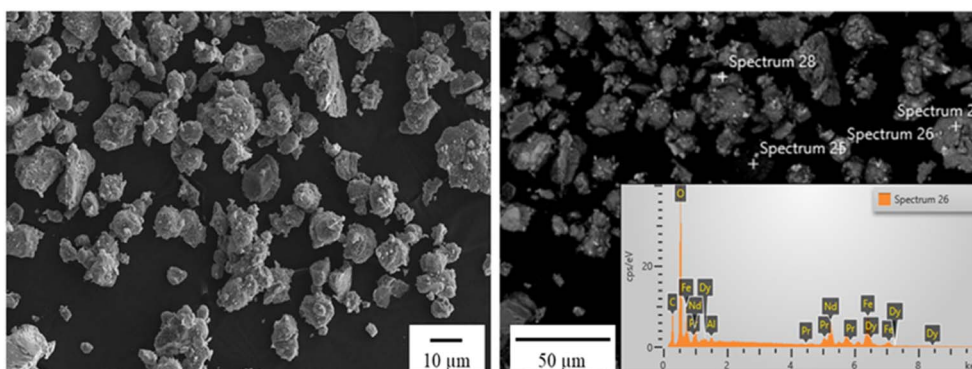

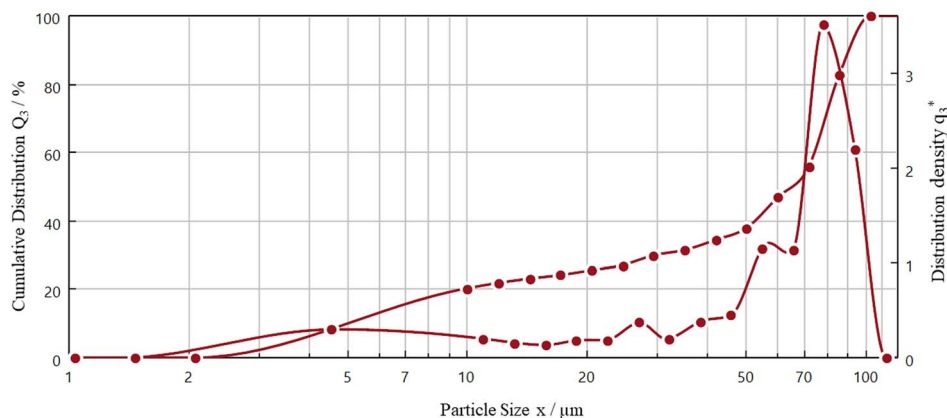Fig. 7 SEM images of the oxidized NdFeB magnet powders with EDS analysis.

Fig. 8 Dynamic particle analysis of the oxidized NdFeB magnet powders.

Table 5 Experimental parameters for selective leaching and results of experiments based on L9 orthogonal arrays

Code	Molar. of acid (mol L^{-1})	S/L ratio	Temperature (°C)	Stirring speed (rpm)	Leach. Eff. [Fe]	S/N for Fe (db)	Leach. Eff. [REE]	S/N for REEs (db)
L1	1	1 : 10	RT	200	19.7	−5.88	255	48.13
L2	1	1 : 30	40	350	60.5	−15.63	170	44.60
L3	1	1 : 50	60	500	218	−26.76	205	46.23
L4	2	1 : 10	40	500	162	−24.19	523	54.37
L5	2	1 : 30	60	200	915	−39.22	515	54.23
L6	2	1 : 50	RT	350	<1	20.0	57	35.11
L7	3	1 : 10	60	350	2530	−48.06	1457	63.26
L8	3	1 : 30	RT	500	12.2	−1.727	115	41.21
L9	3	1 : 50	40	200	157	−23.91	178	45.00

Table 6 ANOVA results for extraction of REEs

Parameter	DoF	SS	MS	F-value
Acid concentration	2	18.491	9.246	
Solid/liquid ratio	2	266.863	133.431	
Temperature	2	257.132	128.566	
Stirring speed	2	5.715	2.858	
Total	8	548.201		

selective leaching parameters, the level of experiments and chemical analysis results determined by ICP analysis. The S/N ratios for REEs and iron were calculated. Table 5 presents the S/N ratio values for each experiment.

F-values, MS, and SS values can be determined by statistical analysis. Tables 6 and 7 represent the calculated values for the extraction of REEs and the extraction of Fe, respectively. Tables

8 and 9 represent the calculated values with *F*-value for the extraction of REEs and the extraction of iron, respectively.

The *F*-value illustrates the effect of the leaching parameters on leaching efficiency. Statistical analysis revealed that process temperature and S/L are the important parameters for the leaching efficiency of REEs, and temperature is the most important parameter for theextraction of iron under the working conditions.

Table 8 ANOVA results for extraction of iron

Parameter	DoF	SS	MS	F-value
Acid concentration	2	176.34	88.17	
Solid/liquid ratio	2	376.38	188.19	
Temperature	2	2701.67	1350.83	
Stirring speed	2	110.01	55.01	
Total	8	3364.4		

Table 7 ANOVA results for extraction of REEs

Parameter	DoF	SS	MS	F-value
Solid/liquid ratio	2	266.863	133.431	0.0069
Temperature	2	257.132	128.566	0.0074
Stirring speed	2	24.207	6.052	
Total	8	555.594		

Table 9 ANOVA results for extraction of iron

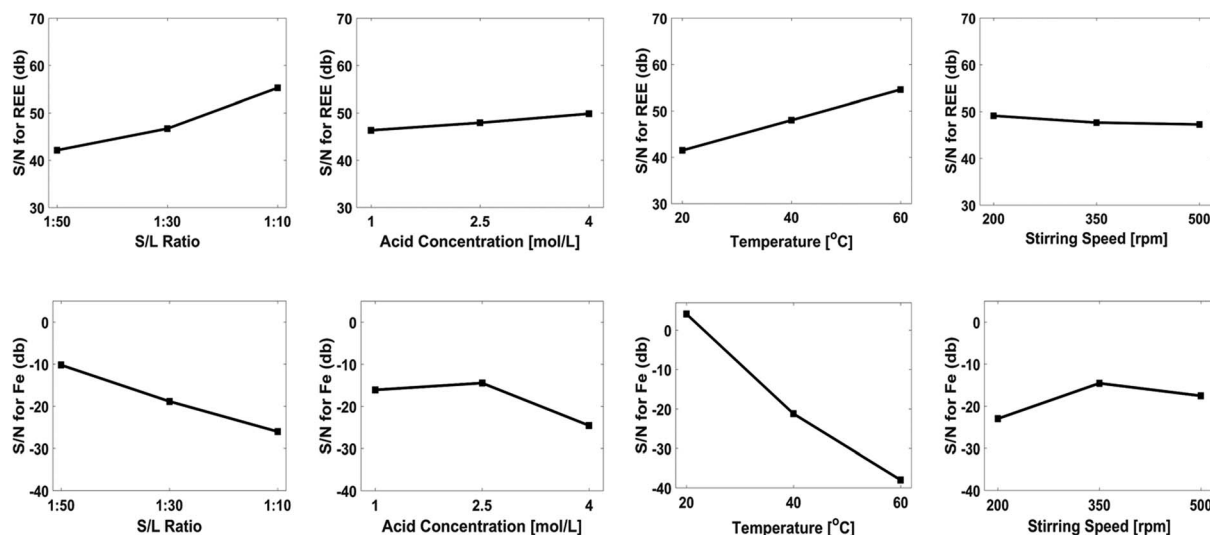| Parameter	DoF	SS	MS	F-value
Solid/liquid ratio	2	376.38	188.19	0.1867
Temperature	2	2701.6	1350.8	0.0092
Error	4	286.35	71.59	
Total	8	3364.4		

Fig. 9 Effect of leaching parameters on the optimization criteria for both REEs and iron.
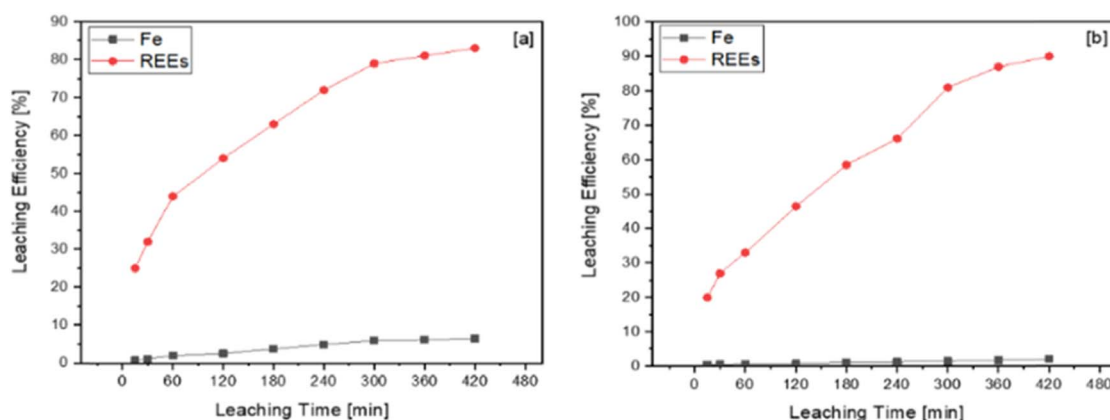

Fig. 10 Effect of leaching time on the leaching efficiency of iron and REEs in (a) 4 mol L^{-1} and (b) 1 mol L^{-1} of nitric acid solution.

Fig. 9 illustrates the effect of the leaching parameters on the optimization criteria for both REEs and iron. According to the Taguchi plots, NdFeB magnet powders should be leached in 4 mol L^{-1} of nitric acid solution with a S/L ratio of 1 : 10 and a stirring speed of 200 rpm at a process temperature of 60 °C, with the goal of achieving maximum REEs content in the leach liquor. On the other hand, the magnet powders should be leached in 2.5 mol L^{-1} of acid concentration with a solid/liquid ratio of 1 : 50 and stirring speed of 350 rpm at a process temperature of 20 °C, with the aim of achieving minimum iron extraction. Validation experiments were conducted under the specified experimental conditions. The aim of this study is to achieve maximum dissolution of REEs. Afterwards, an iron removal process will be performed to obtain high-purity REEs solution. Although 4 mol L^{-1} nitric acid concentration was the best parameter, there is not much difference in the Taguchi plots between 1 mol L^{-1} and 4 mol L^{-1} of acid concentration. Two validation experiments were performed in a 1 mol L^{-1} and a 4 mol L^{-1} nitric acid

solution to compare their effect on REEs and iron dissolution. It was observed that there is no notable difference between 1 mol L^{-1} and 4 mol L^{-1} of nitric acid solution on the dissolution of REEs.

To understand the effect of leaching time on leaching efficiency of iron and REEs, validation experiments were conducted in 1 mol L^{-1} and 4 mol L^{-1} nitric acid solution for 7 h. The chemical analysis results were elucidated, and leaching efficiency of iron and REEs was calculated. Fig. 10a and b show the effect of leaching time on leaching efficiency of iron and REEs in 4 mol L^{-1} of nitric acid solution and 1 mol L^{-1} of nitric acid solution, respectively.

While the duration of leaching showed a minor effect on the leaching efficiency of iron, it showed a major effect on the leaching efficiency of REEs. The dissolution ratio of iron in 4 mol L^{-1} nitric acid solution was higher than in 1 mol L^{-1} nitric acid solution. The leaching efficiency of REEs in 1 mol L^{-1} and 4 mol L^{-1} of nitric acid solution were approximately 90% and 82%, respectively. REEs dissolution was

Table 10 Kinetic models and calculated R^2 values for REEs leaching

| Kinetic models	R^2			k		
	20 °C	40 °C	60 °C	20 °C	40 °C	60 °C
Mixed controlled $-\ln(1-x)$	0.9845	0.9238	0.946	0.0005	0.0007	0.0078
Diff. through product layer $1-(2/3 \times x) - (1-x)^{2/3}$	0.9981	0.9443	0.9423	0.00001	0.00004	0.0007
Chemical reaction control $1-(1-x)^{1/3}$	0.9831	0.9195	0.9814	0.0001	0.0002	0.0017
Surface reaction control by shrinking core model $1-(1-x \times 0.45)^{1/3}$	0.9814	0.9137	0.9957	0.00006	0.00008	0.0004
Shrinking core model $1-(1-x)^{2/3}$	0.9816	0.915	0.996	0.0003	0.0003	0.0023
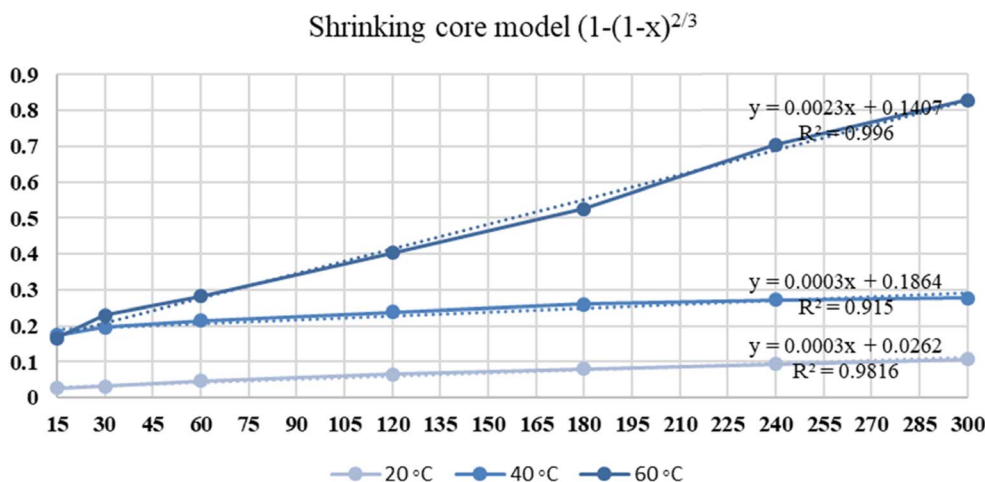
Fig. 11 Kinetic curve of nitric acid leaching of REEs.

inhibited by a solubility limit in 4 mol L^{-1} of the nitric acid solution because iron dissolution ratio in 4 mol L^{-1} of nitric acid solution is higher than in 1 mol L^{-1} of the nitric acid solution.

The leaching of NdFeB magnet powders in 1 mol L^{-1} of nitric acid was analyzed by different kinetic models at different temperatures. Table 10 shows the kinetic models and calculated R^2 values for REEs leaching.

Fig. 12 $\ln k - 1/T$ plots for REEs.

The maximum R^2 values for REEs dissolution are achieved when the shrinking core model is used. Fig. 11 illustrates the kinetic curve of nitric acid leaching of REEs.

The activation energy of the leaching reaction was calculated on the basis of Arrhenius eqn (5).

$$\ln k = \ln A - \frac{E_A}{R + T} \qquad (5)$$

E_a, R and T represent activation energy (kJ mol^{-1}), gas constant (8.314 J mol^{-1}) and temperature (K), respectively. Fig. 12 shows $\ln k - 1/T$ plots for REEs. Adjusted R^2 is approximately 0.5, and R^2 is approximately 0.78.

The activation energy was calculated as 40.375 kJ mol^{-1} for REEs leaching with HNO$_3$.

Characterization of the leach residue

Table 11 shows the XRF analysis of the leach residue obtained from validation experiments performed with 1 mol L^{-1} of nitric acid solution.

Table 11 Chemical analysis of the leach residue obtained from validation experiment

Composition	Co	Fe	Nd	Pr	others, oxides
%	0.17	77.9	1.98	0.71	19.24

Table 12 Box–Behnken matrix and the results concerning the percentage of iron and REEs content in the leach liquor after iron precipitation in the autoclave

Sample	Process temperature [°C]	Time [h]	Water addition [vol%]	Recovery rate of REEs %	Removal rate of iron %
A1	160	6	0	99.13	0.63
A2	180	6	25	94.64	0.15
A3	180	4	0	96.27	0.52
A4	180	4	50	91.61	0.02
A5	160	2	50	92.13	0.09
A6	180	2	25	96.54	0.31
A7	140	2	25	93.34	2.09
A8	160	4	25	94.12	0.35
A9	160	6	50	92.30	0.06
A10	140	4	0	96.54	1.52
A11	160	2	0	94.18	1.04
A12	160	4	25	91.35	0.27
A13	160	4	25	93.25	0.30
A14	140	6	25	90.92	0.35
A15	140	4	50	90.57	0.11

Table 13 ANOVA results for REEs precipitation

Source	DF	Adj SS	Adj MS	F-value	P-value
Model	9	67.8754	7.5417	2.03	0.226
Linear	3	58.1677	19.3892	5.22	0.053
Temperature	1	7.4112	7.4112	1.99	0.217
Time	1	0.0036	0.0036	0.00	0.976
Water addition	1	50.7528	50.7528	13.65	0.014
Square	3	4.9120	1.6373	0.44	0.734
Temperature × temperature	1	0.0113	0.0113	0.00	0.958
Time × time	1	2.9769	2.9769	0.80	0.412
Water addition × water addition	1	2.2922	2.2922	0.62	0.468
2-Way interaction	3	4.7957	1.5986	0.43	0.741
Temperature × time	1	0.0676	0.0676	0.02	0.898
Temperature × water addition	1	0.4225	0.4225	0.11	0.750
Time × water addition	1	4.3056	4.3056	1.16	0.331
Error	5	18.5873	3.7175		
Lack-of-fit	3	14.5741	4.8580	2.42	0.306
Pure error	2	4.0133	2.0066		
Total	14	86.4628			

Table 14 ANOVA results for iron precipitation

| Source	DF	Adj SS	Adj MS	F-value	P-value
Model	9	4.52395	0.50266	6.48	0.027
Linear	3	3.33318	1.11106	14.33	0.007
Temperature	1	1.17811	1.17811	15.19	0.011
Time	1	0.68445	0.68445	8.83	0.031
Water addition	1	1.47061	1.47061	18.96	0.007
Square	3	0.32355	0.10785	1.39	0.348
Temperature × temperature	1	0.23619	0.23619	3.05	0.141
Time × time	1	0.10103	0.10103	1.30	0.305
Water addition × water addition	1	0.00108	0.00108	0.01	0.911
2-Way interaction	3	0.86722	0.28907	3.73	0.095
Temperature × time	1	0.62410	0.62410	8.05	0.036
Temperature × water addition	1	0.20702	0.20702	2.67	0.163
Time × water addition	1	0.03610	0.03610	0.47	0.525
Error	5	0.38774	0.07755		
Lack-of-fit	3	0.38448	0.12816	78.46	0.013
Pure error	2	0.00327	0.00163		
Total	14	4.91169			
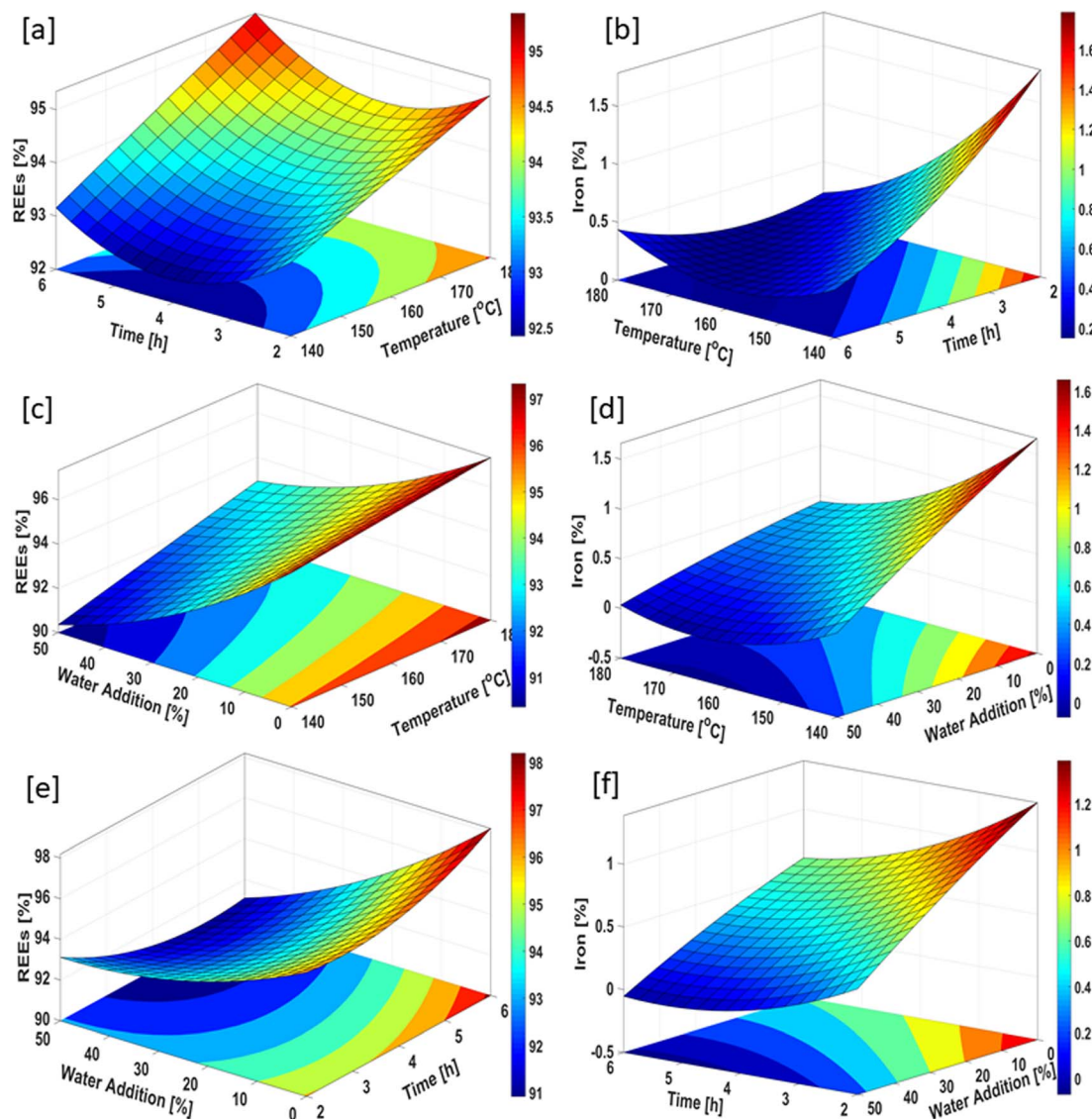
Fig. 13 Three-dimensional response surface counter plots for (a and b) the effect of time and temperature, (c and d) the effect of water addition and temperature, and (e and f) the effect of water addition and time.

The amount of Fe, Nd, and Pr were 77.9%, 1.98%, and 0.71% of the leach residue, respectively.

Iron precipitation in the autoclave

The iron dissolved during the selective leaching was precipitated in the autoclave. The iron precipitation experiments were performed on the basis of the Box–Behnken design. The significant experimental parameters affecting the efficiency of iron removal under pressure and temperature in the autoclave were determined by ANOVA analysis. The precipitation process was optimized with RSM, which results in the minimum iron and maximum REEs content in the leach liquor. Table 12 shows the Box–Behnken matrix and the results concerning the percentage of iron and REEs content in the leach liquor after iron precipitation in the autoclave.

Model fitting, statistical analysis and response surface analysis

The empirical relationship between the input parameters (temperature T, time TM, and water addition W) and the output variables was examined through regression analysis. The equations for the precipitation of REEs and iron are given in eqn (6) and (7), respectively.

$$\text{REEs} = 98.2 - 0.025T - 1.79\text{TM} - 0.185W + 0.00014T \times T + 0.224\,\text{TM} \times \text{TM} + 0.00126W \times W + 0.0032T \times \text{TM} + 0.00065T \times W - 0.0207T \times W \quad (6)$$

$$\text{Fe} = 29.55 - 0.272T - 2.105\text{TM} - 0.0962W + 0.000632T \times T + 0.0414\text{TM} \times \text{TM} + 0.000027W \times W + 0.00987T \times \text{TM} + 0.000455T \times W + 0.00190\text{TM} \times W \quad (7)$$

Eqn (6) provides the regression equation for the precipitation of REEs, which has $R^2 = 78.50\%$ and R^2-adjusted $= 39.81\%$. Moreover, eqn (7) provides the regression equation for iron precipitation, which has $R^2 = 92.11\%$ and R^2-adjusted $= 77.90\%$. ANOVA was carried out for the precipitation of iron and REEs.

The F-value for each parameter presents the influence of the precipitation parameters on the purity of the solution. A P-value of less than 0.05 indicates the statistical significance of each process parameter. Tables 13 and 14 provide the MS, SS, F-value, and P-value of process parameters for REEs and iron, respectively.

Statistical analysis revealed that while water addition is the most important parameter for the precipitation of REEs, temperature, time and water addition are the significant parameters for the removal of iron in the autoclave under the experimental working conditions. Fig. 13 illustrates the surface response and contour plots for determining the maximum REEs and minimum iron content in the leach liquor.

The main purpose of this step is to achieve REEs with high purity in the leach liquor. The efficiency of REEs recovery needs to be increased by means of defining the optimal process parameters for iron removal in the autoclave. Fig. 13 illustrates the surface response and contour plots for determining the maximum REEs and minimum iron contents in the leach liquor.

Fig. 13a presents the surface response and contour plot for the effect of time and temperature on the maximum REEs content. This figure illustrates that REEs with high purity can be achieved when the process temperature is higher than 170 °C and the time is longer than 5 h. Fig. 13b shows the effect of time and temperature on the minimum iron content in the leach liquor. A process time higher than 5 h and a temperature higher than 160 °C provide the minimum iron content in the leach liquor after autoclave experiment. Fig. 13c and d illustrate the effect of temperature and water addition on maximum REEs

and minimum iron contents in the leach liquor, respectively. A process temperature higher than 170 °C and water addition of 0% provide the maximum REEs content. As can be seen in Fig. 13d, low iron values in the leach liquor were obtained for the temperature values of 165 °C < T < 180 °C and at the water addition of 35%. Fig. 13e displays the effect of water addition and time on achieving the maximum REEs content in the leach liquor. This figure shows that the maximum content of REEs in the leach liquor was obtained at lower water addition and higher process time. Fig. 13f illustrates that low iron content in the leach liquor was achieved at the water addition of 50% and time period of 4 h < TM < 6 h. These surface response and contour plots display that temperature, water addition and time are defined as important parameters for promising results of the iron removal process. This conclusion is also consistent with the ANOVA results for the iron removal process in the autoclave.

Optimization of the iron precipitation process in the autoclave

This optimization process aims to achieve high purity REEs in the leach liquor while preventing the precipitation of REEs together with iron. Therefore, both a maximum REEs content and a minimum iron content are anticipated during the iron removal process in the autoclave. For this purpose, an optimization study was conducted with MINITAB. The optimization plot for both maximum REEs and minimum iron content is presented in Fig. 14.

The optimal parameters were determined to be a process temperature of approximately 175 °C, a process time of 6 h, and a water addition of 0%. A validation experiment was conducted
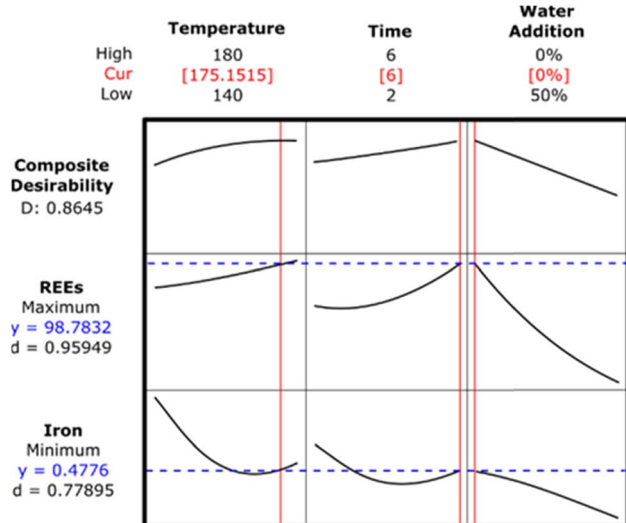

Fig. 14 Optimization plots for maximum REEs and minimum iron content in the leach liquor.
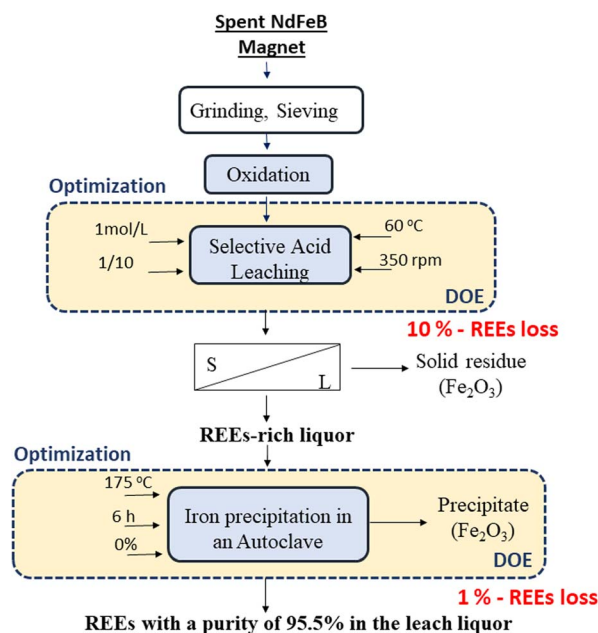

Fig. 15 Proposed conceptual flowchart for high REEs recovery from spent NdFeB magnets.

with the specified process parameters. Iron was removed from the system with 1% loss of REEs.

Fig. 15 illustrates the proposed conceptual flowsheet for high REEs recovery from the spent NdFeB magnets.

Conclusion

In this study, magnet powders were oxidized at 900 °C followed by a selective leaching process. The iron extracted during leaching was removed through iron hydrolysis in the autoclave.

Notable findings of this study are given as follows: the Taguchi method was employed to determine the optimal leaching parameters for maximum REEs extraction and minimum iron extraction. Statistical analysis revealed that while process temperature and S/L are the important parameters for the leaching efficiency of REEs, temperature is the most important parameter for the dissolution of iron under the experimental working conditions.

The aim of this study was to achieve maximum dissolution of REEs. Afterwards, the iron removal process was performed to obtain high-purity REEs solution. Although 4 mol L^{-1} nitric acid concentration was the best parameter, there was not much difference in the Taguchi plots between 1 mol L^{-1} and 4 mol L^{-1} acid concentrations. Thus, the optimal nitric acid concentration was chosen as 1 mol L^{-1}.

The iron extracted during leaching was removed in the autoclave under pressure. The precipitation experiments were carried out based on the Box–Behnken experimental design.

The validation experiment was performed at a process temperature of 175 °C, a process time of 6 h, and a water addition of approximately 0%. Thus, iron was removed from the system with 1% loss of REEs.

Author contributions

Conceptualization E. E. K., experiment E. E. K., B. P. Data curation E. E. K., formal analysis E. E. K., funding acquisition S. S., S. G., B. F., investigation E. E. K., methodology E. E. K, project administration S. S., S. G., B. F., resources S. S., S. G., B. F., supervision S. G. and B. F., validation E. E. K., writing – original draft E. E. K., writing – review and editing E. E. K., B. P., S. S., S. G., B. F.

Conflicts of interest

There are no conflicts to declare.

Acknowledgements

References

1 K. T. Rim, Effects of rare earth elements on the environment and human health: a literature review, *J. Toxicol. Environ. Health Sci.*, 2016, **8**(3), 189–200.

2 U. K. Mudali, M. Patil, R. Saravanabhavan and V. K. Saraswat, Review on E-waste Recycling: Part II—Technologies for Recovery of Rare Earth Metals, *Trans. Indian Natl. Acad. Eng.*, 2021, 1–19.

3 L. Silvestri, A. Forcina, C. Silvestri and M. Traverso, Circularity potential of rare earths for sustainable mobility: Recent developments, challenges and future prospects, *J. Cleaner Prod.*, 2021, **292**, 126089.

4 E. Lewicka, K. Guzik and K. Galos, On the Possibilities of Critical Raw Materials Production from the EU's Primary Sources, *Resources*, 2021, **10**(5), 50.

5 D. Gielen and M. Lyons, Critical materials for the energy transition, *Rare Earth Elem.*, 2022, 3–45.

6 K. Binnemans and P. T. Jones, Rare earths and the balance problem, *J. Sustain. Metall.*, 2015, **1**(1), 29–38.

7 M. V. Reimer, H. Y. Schenk-Mathes, M. F. Hoffmann and T. Elwert, Recycling decisions in 2020, 2030, and 2040—when can substantial NdFeB extraction be expected in the EU, *Metals*, 2018, **8**(11), 867.

8 R. Schulze and M. Buchert, Estimates of global REE recycling potentials from NdFeB magnet material, *Resour. Conserv. Recycl.*, 2016, **113**, 12–27.

9 Y. Yang, A. Walton, R. Sheridan, K. Güth, R. Gauß, O. Gutfleisch and K. Binnemans, REE recovery from end-of-life NdFeB permanent magnet scrap: a critical review, *J. Sustain. Metall.*, 2017, **3**(1), 122–149.

10 S. Kruse, K. Raulf, T. Pretz and B. Friedrich, Influencing factors on the melting characteristics of NdFeB-Based production wastes for the recovery of rare earth compounds, *J. Sustain. Metall.*, 2017, **3**(1), 168–178.

11 S. Kruse, K. Raulf, A. Trentmann, T. Pretz and B. Friedrich, Processing of grinding slurries arising from NdFeB magnet production, *Chem. Ing. Tech.*, 2015, **87**(11), 1589–1598.

12 E. G. Polyakov and A. S. Sibilev, Recycling rare-earth-metal wastes by pyrometallurgical methods, *Metallurgist*, 2015, **59**(5), 368–373.

13 H. Chung, S. Stopic, E. Emil-Kaya, S. Gürmen and B. Friedrich, Recovery of Rare Earth Elements from Spent NdFeB-Magnets: Separation of Iron through Reductive Smelting of the Oxidized Material (Second Part), *Metals*, 2022, **12**(10), 1615.

14 S. Stopic, B. Polat, H. Chung, E. Emil-Kaya, S. Smiljanić, S. Gürmen and B. Friedrich, Recovery of Rare Earth Elements through Spent NdFeB Magnet Oxidation (First Part), *Metals*, 2022, **12**(9), 1464.

15 Y. Zhang, A. F. Gu, Z. Su, S. Liu, C. Anderson and T. Jiang, Hydrometallurgical Recovery of Rare Earth Elements from NdFeB Permanent Magnet Scrap: A Review, *Metals*, 2020, **10**(6), 841.

16 E. Emil-Kaya, S. Stopic, S. Gürmen and B. Friedrich, Production of rare earth element oxide powders by

solution combustion: a new approach for recycling of NdFeB magnets, *RSC Adv.*, 2022, **12**(48), 31478–31488.

17 L. Omodara, S. Pitkäaho, E. M. Turpeinen, P. Saavalainen, K. Oravisjärvi and R. L. Keiski, Recycling and substitution of light rare earth elements, cerium, lanthanum, neodymium, and praseodymium from end-of-life applications-A review, *J. Cleaner Prod.*, 2019, **236**, 117573.

18 E. Uysal, S. Al, E. Emil-Kaya, S. Stopic, S. Gürmen and B. Friedrich, Hydrometallurgical recycling of waste NdFeB magnets: design of experiment, optimisation of low concentrations of sulphuric acid leaching and process analysis, *Can. Metall. Q.*, 2022, 1–12.

19 A. Akcil, Y. A. Ibrahim, P. Meshram, S. Panda and A. Abhilash, Hydrometallurgical recycling strategies for recovery of rare earth elements from consumer electronic scraps: a review, *J. Chem. Technol. Biotechnol.*, 2021, 1785–1797.

20 C. Tunsu, M. Petranikova, C. Ekberg and T. Retegan, A hydrometallurgical process for the recovery of rare earth elements from fluorescent lamp waste fractions, *Sep. Purif. Technol.*, 2016, **161**, 172–186.

21 S. Peelman, Z. H. Sun, J. Sietsma and Y. Yang, Leaching of rare earth elements: review of past and present technologies, *Rare Earths Industry*, 2016, 319–334.

22 A. Kumari, M. K. Sinha, S. Pramanik and S. K. Sahu, Recovery of rare earths from spent NdFeB magnets of wind turbine: Leaching and kinetic aspects, *Waste Manage.*, 2018, **75**, 486–498.

23 A. C. Ni'am, Y. F. Wang, S. W. Chen and S. J. You, Recovery of rare earth elements from waste permanent magnet (WPMs) *via* selective leaching using the Taguchi method, *J. Taiwan Inst. Chem. Eng.*, 2019, **97**, 137–145.

24 Y. Jiang, Y. Deng, W. Xin and C. Guo, Oxidative Roasting–Selective Pressure Leaching Process for Rare Earth Recovery from NdFeB Magnet Scrap, *Trans. Indian Inst. Met.*, 2020, 1–9.

25 H. S. Yoon, C. J. Kim, K. W. Chung, S. J. Lee, A. R. Joe, Y. H. Shin and J. G. Kim, Leaching kinetics of neodymium in sulfuric acid from E-scrap of NdFeB permanent magnet, *Korean J. Chem. Eng.*, 2014, **31**(4), 706–711.

26 F. Liu, A. Porvali, J. Wang, H. Wang, C. Peng, B. P. Wilson and M. Lundström, Recovery and separation of rare earths and boron from spent Nd-Fe-B magnets, *Miner. Eng.*, 2020, **145**, 106097.

27 F. Mao, N. Zhu, W. Zhu, B. Liu, P. Wu and Z. Dang, Efficient recovery of rare earth elements from discarded NdFeB magnets by mechanical activation coupled with acid leaching, *Environ. Sci. Pollut. Res.*, 2021, 1–12.

28 J. E. Dutrizac and P. A. Riveros, The precipitation of hematite from ferric chloride media at atmospheric pressure, *Metall. Mater. Trans. B*, 1999, **30**(6), 993–1001.

29 T. C. Cheng, G. P. Demopoulos, Y. Shibachi and H. Masuda, The precipitation chemistry and performance of the Akita hematite process—an integrated laboratory and industrial scale study, *Electrometall. Environ. Hydrometallurgy*, 2013, **2**, 1657–1674.